The Astrophysical Journal, 996:44 (12pp), 2026 January 1 https://doi.org/10.3847/1538-4357/ae2029

21 cm Signal from the Thermal Evolution of Lyα during Cosmic Dawn

Janakee Raste[1] and Shiv K. Sethi[2]
[1] National Centre for Radio Astrophysics, Tata Institute of Fundamental Research, Pune 411007, India; janakee@ncra.tifr.res.in
[2] Raman Research Institute, Bengaluru 560080, India
Received 2025 June 15; revised 2025 October 27; accepted 2025 November 13; published 2025 December 23

Abstract

The Lyα photons couple the spin temperature of neutral hydrogen (H I) to the kinetic temperature during the era of cosmic dawn (CD). During this process, they also exchange energy with the medium, heating and cooling the H I. In addition, we expect X-ray photons to heat the mostly neutral gas during this era. We solve this coupled system (Lyα–H I system along with X-ray heating) for a period of 500 Myr (redshift range $8 < z < 25$). Our main results are: (a) Without X-ray heating, the temperature of the gas reaches an equilibrium, which is nearly independent of photon intensity and only weakly dependent on the expansion of the Universe. The main determinant of the quasi-static temperature is the ratio of injected and continuum Lyα photons. (b) While X-ray photons provide an additional source of heating at initial times, for large enough Lyα photon intensity, the system tends to reach the same quasi-static temperature as expected without additional heating. This limit is reached when the density of photons close to the Lyα resonance far exceeds the H I number density. (c) We compute the global H I signal for these scenarios. In the limit of the large density of Lyα photons, the spin temperature of the hyperfine line is fixed. This freezes the global H I signal from the era of CD and the crossover redshift from absorption to emission. This feature depends only on the ratio of injected to continuum Lyα photons, and the global H I signal can help us determine this ratio.

Unified Astronomy Thesaurus concepts: Reionization (1383); Cosmology (343); H I line emission (690); Intergalactic medium (813)

1. Introduction

H I cosmology has emerged as an important area of cosmology research in the past two decades. Its main appeal arises from the fact that the redshifted H I line can be used to study three important eras—dark ages ($200 \lesssim z \lesssim 35$), cosmic dawn (CD; $35 \lesssim z \lesssim 15$), and Epoch of Reionization (EoR; $15 \lesssim z \lesssim 6$)—which are not easily accessible to other cosmological probes. Our current partial understanding of these eras is based on the Gunn–Peterson (GP) test on high-redshift quasars at $z \simeq 6$ (X. Fan et al. 2000; R. H. Becker et al. 2001) and the detection of cosmic microwave background (CMB) temperature and polarization anisotropies from the Wilkinson Microwave Anisotropy Probe and Planck satellite missions (G. Hinshaw et al. 2013; Planck Collaboration et al. 2020). Most recent Planck results determine the EoR, $z_{\rm reion} = 7.75 \pm 0.73$. These probes suggest that the Universe might have made a transition from fully neutral to highly ionized in the redshift range $6 < z < 10$. These results are supplemented by recent Lyα forest observations, which suggest that the EoR might have ended at $z \simeq 5.3$ (G. Kulkarni et al. 2019; G. D. Becker et al. 2021; J. Raste et al. 2021; S. E. I. Bosman et al. 2022; Y. Zhu et al. 2023).

The current theoretical paradigm, based on the ΛCDM model, suggests that the dark ages ended around $z \simeq 30$ with the formation of the first objects in the Universe. These subgalactic structures emitted UV and X-ray radiation into the medium, which heated and ionized the gas, while also coupling the Lyα radiation to the H I level population. For the redshift range, $10 \lesssim z \lesssim 30$, the global ionized fraction is small, but it increases rapidly for smaller redshifts, ending the EoR at $z \simeq 6$ (R. Barkana & A. Loeb 2001; M. F. Morales & J. S. B. Wyithe 2010; J. R. Pritchard & A. Loeb 2012; A. Natarajan & N. Yoshida 2014). Although this paradigm is generally accepted, we currently lack detailed information on the physics of the first stars and galaxies, a situation that has become even more complex with JWST results (H. Yan et al. 2022; S. Hassan et al. 2023).

The redshifted 21 cm signal from the era of CD/EoR is determined by three radiation fields: hydrogen-ionizing photons, photons in the frequency range between Lyα and Lyman-limit (referred to as "Lyα" radiation, this radiation couples Lyα photons to H I hyperfine levels through the Wouthuysen–Field effect), and X-ray radiation (photons in the approximate energy range 100 eV–10 keV, whose main role is to heat the neutral gas; e.g., S. K. Sethi 2005; S. R. Furlanetto et al. 2006; J. R. Pritchard & A. Loeb 2012; J. Raste & S. Sethi 2018, 2019 and references therein).

In this paper, we investigate the thermal impact of Lyα photons. This is a less studied aspect of Lyα photons because the number density of Lyα needed for Wouthuysen–Field coupling is too small to have a significant thermal impact (X. Chen & J. Miralda-Escudé 2004; see also P. Madau et al. 1997). This claim has since been confirmed by other authors (e.g., L. Chuzhoy & P. R. Shapiro 2006, 2007; C. M. Hirata 2006; A. Meiksin 2006; J. R. Pritchard & S. R. Furlanetto 2006; G. B. Rybicki 2006; see also T. Venumadhav et al. 2018; R. Ghara & G. Mellema 2020; A. Meiksin & P. Madau 2021; S. Mittal & G. Kulkarni 2021; I. Reis et al. 2021; J. B. Munoz et al. 2022; B. Semelin et al. 2023; H. Shimabukuro et al. 2023; S. Mittal et al. 2024). In J. Raste et al. (2024; hereafter Paper I), we studied this issue as an initial value problem and solved the simultaneous evolution of Lyα spectral profile and the gas temperature. Many initial

profiles (injected, continuum, and a mix of the two) were considered. It was shown that both the spectral profile and the gas temperature reach quasi-equilibrium on timescales that depend on the photon injection rate. For large photon injection rates, this timescale is less than a few million years. While Paper I focused on a detailed theoretical analysis, our aim in this paper is to extend this analysis to enable us to compute cosmological observables.

In Paper I, the coupled photon-gas system was evolved to a few million years, but this only allowed us to understand the equilibrium states for large photon injection rates. In this paper, we evolve the system to nearly half a billion years, which enables us to treat small photon injection rates adequately, clearly discern the effect of expansion of the Universe, and reliably compute the cosmological observables. Second, we include X-ray heating as an additional source in our work. In the usual analysis, Lyα and X-ray photons are treated as uncoupled. However, our analysis shows that they are strongly coupled for a large Lyα injection rate. Third, this enables us to compute the global H I signal during the CD/EoR eras. In particular, our analysis reveals the striking impact of Lyα and X-ray coupling on the observed H I signal.

In the next section, we discuss our formalism in brief and defer to Paper I for a more detailed discussion. In Section 3, we show the long-term evolution of the photon profile and gas temperature. In Section 4, we study the implications of X-ray heating within the framework of many models of Lyα and X-ray injection. The global H I signal is also computed for these models. Finally, in Section 5, we summarize our results and provide possible future avenues of our work. Throughout the paper, we assume the best-fit Planck parameters corresponding to the spatially flat FRW Universe: $\Omega_c h^2 = 0.12$ and $\Omega_b h^2 = 0.0224$ (Planck Collaboration et al. 2020).

2. Thermal Coupling of Lyα Photons with H I: X-Ray Heating

In Paper I, we developed the formalism to determine the thermal coupling of Lyα photons and neutral hydrogen. We give here only the equations directly relevant for this work and refer the reader to Paper I for more details.

Our aim is to solve for the evolution of the photon occupation number in an FRW Universe. Let $J(\hat{n}, \nu, t) \equiv dN/(d\nu dV d\Omega)$ denote the number density of photons in the frequency range ν and $\nu + d\nu$, traveling in a direction $\hat{n}$. It is more convenient to work with variable $x = (\nu - \nu_\alpha)/\Delta\nu_D$, where $\Delta\nu_D = \nu_\alpha v_T/c$ is the Doppler width with thermal velocity $v_T = \sqrt{2kT_K/m_p}$. This allows us to define $J(x, t) = J(\nu, t)\Delta\nu_D$. $J(x, t)$ is the number density of photons per unit solid angle in the frequency range corresponding to x and $x + dx$. The evolution of $J(x, t)$ can be written as (for details, see Paper I and references therein):

$$\frac{1}{a^3}\frac{\partial(J(x,t)a^3)}{\partial t'} = \frac{\partial}{\partial x}\left[\frac{\phi(x)}{2}\frac{\partial J(x,t)}{\partial x} + (\eta\phi(x) + \gamma)J(x,t)\right] + C'\psi(x). \quad (1)$$

Here, the dimensionless time is defined as $t' = t/t_{sca}$, where $t_{sca} = 1/(n\sigma_0 c(1 + w/T_K))$ is the the scattering time at the line center. The parameter $w = b\nu_{21}^2 m_p c^2/(2\nu_\alpha^2 k)$, which captures the contribution of hyperfine energy exchange, is small ($w \simeq 0.4$ K), and the impact of hyperfine energy exchange is negligible except at very low temperatures. $\sigma_0 = (3/8\pi)(\lambda_\alpha^2 A_\alpha/\Delta\nu_D)$ is the Lyα scattering cross section at the line center. The Sobolev parameter $\gamma = \tau_{GP}^{-1}(1 + w/T_K)^{-1}$ compares the relative efficacy of scattering and expansion, with the GP optical depth $\tau_{GP} = \sigma_0 n v_T/H$. The recoil parameter $\eta = (1 + w/T_S)(1 + w/T_K)^{-1}(h\nu_\alpha/(2kT_K m_p c^2)^{1/2})$. C' is the rescaled photon injection rate: $C' = C/(n\sigma_0 c(1 + w/T_K))$; C is the rate at which the new photons are injected. For our work, we define C as the number density of new photons that are produced per unit time per unit solid angle in the frequency range from Lyα to the Lyman limit (in cm^{-3} s^{-1} sr^{-1}). $\psi(x)$, the normalized photon injection profile, is defined such that $\int\psi(x)dx = 1$.

To compute relevant variables, we need the spin temperature, T_S, which can be expressed as:

$$T_S = \frac{T_{CMB} + y_c T_K + y_\alpha T_\alpha}{1 + y_c + y_\alpha}, \quad (2)$$

and T_α, the color temperature close to the resonance line is,

$$T_\alpha = -\frac{h(\nu - \nu_\alpha)}{k\ \ln\left(\frac{J(\nu)}{J(\nu_\alpha)}\right)}. \quad (3)$$

The Lyα coupling coefficient,

$$y_\alpha = (h\nu_{21}/kT_\alpha)(P_{21}/A_{21}), \quad (4)$$

with the rate of deexcitation of the upper hyperfine level, $P_{21} = (4/27)P_\alpha$ and $P_\alpha \simeq 4\pi\sigma_0 J(\nu_\alpha)c$ (see, e.g., G. B. Field 1958; M. F. Morales & J. S. B. Wyithe 2010 for more details). In thermal equilibrium between Lyα photons and the intergalactic medium (IGM), $T_\alpha = T_K$. If $y_\alpha \gg y_c$ and $y_\alpha \gg 1$, then $T_S = T_\alpha$.

We further redefine $J(x, t) \rightarrow a^3 J(x, t)$ and $C' \rightarrow C'a^3$, converting the photon intensity and the photon production rate into comoving quantities. This gives us,

$$\frac{\partial J(x,t)}{\partial t'} = \frac{\partial}{\partial x}\left[\frac{\phi(x)}{2}\frac{\partial J(x,t)}{\partial x} + (\eta\phi(x) + \gamma)J(x,t)\right] + C'\psi(x). \quad (5)$$

This equation is similar to the one derived by G. B. Rybicki & I. P. dell'Antonio (1994) with two key differences: it includes a factor of a^3 instead of a^2, and it correctly accounts for energy exchange owing to hyperfine mixing. It can be readily shown that $C't' = Ct$ is the photon number density integrated over all frequencies, which is consistent with the conservation of the number of photons.

The evolution of $J(x)$ and the spin temperature, T_S, is determined by the thermal state of the gas. The evolution of kinetic temperature T_K for a neutral, monoatomic gas is given by:

$$\frac{dT_K}{dt} = -2HT_K + \frac{2}{3}\frac{(\dot{q}_\alpha + \dot{q}_{xray})}{n_b k}. \quad (6)$$

Here, $\dot{q}_{xray}$ is the energy injection owing to X-ray photons and $\dot{q}_\alpha = \dot{Q}n_b$ is the rate at which the energy is injected by Lyα photons per unit volume (erg cm^{-3} s^{-1}; for details see Paper I),

with:

$$\dot{Q} = 4\pi c \int \frac{(h\nu_\alpha)^2}{m_p c^2}\sigma_0\phi(x)\left(J(x,t) + \frac{kT_K}{\Delta\nu_D h}J'(x,t)\right)dx + 4\pi c \int \frac{b(h\nu_{21})^2}{2kT_S}\sigma_0\phi(x)\left(J(x,t) + \frac{kT_S}{\Delta\nu_D h}J'(x,t)\right)dx, \quad (7)$$

and $J'(x, t) = dJ/dx$.

Simultaneous solutions to Equations (2), (5), (6), and (7) yield the evolution of the photon profile along with the hyperfine and thermal state of H I.

3. Long-term Evolution

In Paper I, we studied the evolution of intensity profiles for short periods of $t \lesssim 5$ Myr. This timescale suffices for many purposes, e.g., for establishing an approximate equilibrium gas temperature. However, we also showed that photon profiles in some cases (e.g., the continuum and continuum-plus-injected intensity profiles) display long-term evolution. We dealt with these cases by employing a smaller (and unrealistic) value of x_{max}. In this work, we explore the more realistic case, $x_{max} \simeq 10^5$. This requires us to evolve the system for more than 100 million years. The long-term evolution also enables us to study the approach to equilibrium for smaller photon injection rates, C, than was possible in our earlier work.

In Figure 1, we show the long-term evolution of intensity profiles for $x_{max} = 1.4 \times 10^5$, which corresponds to the frequency range between Lyα and Lyman-β. To illustrate the approach to equilibrium profile, one can consider many cases: (a) neglect the expansion of the Universe. Without expansion, the equilibrium profile $\propto \exp(-h(\nu - \nu_\alpha)/(kT))$ (for details, see Paper I and N. Chugai 1980; G. Rybicki & D. Hummer 1994; L. Chuzhoy & P. R. Shapiro 2006), (b) neglect scattering. This case was discussed in detail in Paper I. This allows us to compute the relevant timescales for reaching equilibrium analytically. As we showed in Paper I, these solutions guide us in understanding the equilibrium in realistic cases. In this paper, we consider another approximation to study the dynamics of the coupled system: we include both the scattering and expansion mechanisms but assume a constant expansion rate and no evolution of other relevant quantities, such as number density. This approximation allows us to separate the impact of long-term evolution from the short-term evolution of the system. We evolve the system for close to 100 million years, a period over which both the number density and the expansion rate change substantially. However, by holding these quantities constant, as we show below, we can better understand the quasi-equilibrium states that are reached in shorter times. Therefore, the aim of this approximation is to isolate the impact of different physical processes. We refer to this case as "local approximation."

Figure 1 (lower panels) shows that for the local approximation, a nonevolving intensity profile is reached in nearly 50 million years. In Paper I, we analytically derived the evolution of photon spectra for both injected and continuum profiles for the no-scattering case and argued they give a reasonable approximation of the timescale over which the equilibrium is reached and equilibrium intensity profiles in most realistic cases. Although it is not possible to analytically derive the photon spectra when both injected and continuum photons are present, the equilibrium profiles displayed in the lower panels of Figure 1 are consistent with our general findings of Paper I. In particular, we notice how the flat profile makes a transition to a quasi-static tilted profile, and the tilt moves to a smaller frequency with time. For us, the relevant timescale is the time over which the profile around $x \simeq 0$ becomes tilted; this timescale corresponds to the time over which the photons redshift from $x = x_{max}$ to $x = 0$.

In the upper panels of Figure 1, we show the long-term evolution of the spectral profile when all the relevant physics is included. In this case, we notice that the photon profiles do not relax to a quasi-steady state but keep evolving even after the profile becomes tilted. A comparison with the lower panels based on local approximation shows the main cause of this evolution to be the redshift evolution of the expansion rate and the number density of H I atoms, which becomes important over the long-term evolution of the system. We notice that we did not see this behavior in Paper I because the evolution timescale was much shorter.

In Figure 2, we show the long-term temperature evolution for a range of models. Except for the smallest photon rate, the temperature reaches an equilibrium value in $t \lesssim 100$ Myr. In the local approximation (case (c) above), the temperature reaches the same constant value independent of the photon injection rate, C; this was anticipated in Paper I based on shorter timescales.[3] The thermal evolution for the local approximation is consistent with the corresponding photon profiles in Figure 1, as both the photon profile and the gas temperature reach quasi-steady states. The redshift evolution of relevant quantities causes both the IGM temperature and the intensity profile to slowly evolve. However, Figure 2 shows that the local approximation gives a fairly precise value of the equilibrium temperature.

In the right panel of Figure 2, the evolution of y_α, the parameter that denotes the efficiency of coupling between the spin temperature, T_S, of the 21 cm line and Lyα color temperature, T_α, is shown. The dimensionless parameter y_α increases with the Lyα intensity and is inversely proportional to the color temperature, T_α (Equation (4)). As $T_\alpha = T_K$, the evolution of y_α can be understood from the left panel of Figures 2 and 1. For $y_\alpha > 1$, $T_S \simeq T_\alpha$. The right panel of Figure 2 shows that this coupling becomes efficient over timescales shorter than the expansion timescale for all models we consider. We return to the implications of this in a later section.

4. Impact of X-Ray Heating

During the eras of CD/EoR, the neutral gas is also heated by X-ray photons emitted from ionizing sources. Here, we include the impact of this additional source of heating. In this section, our aim is to discern generic outcomes, so we do not consider specific models based on CD/EoR physics. We consider such models in the next section.

In Figure 3, we show the thermal evolution of the H I gas in the presence of Lyα photons along with another heating source. To capture the full impact of the interaction of the new heating source with the coupled Lyα–H I system, we consider

[3] In Paper I, using a smaller, unrealistic value of x_{max}, we also argued that when the tilted profile is reached at $x = 0$, the equilibrium temperature decreases by a small amount. Here, we verify this result on the basis of long-term thermal evolution. In Figure 2, we notice a small step function in temperature in dashed lines close to 50 Myr.

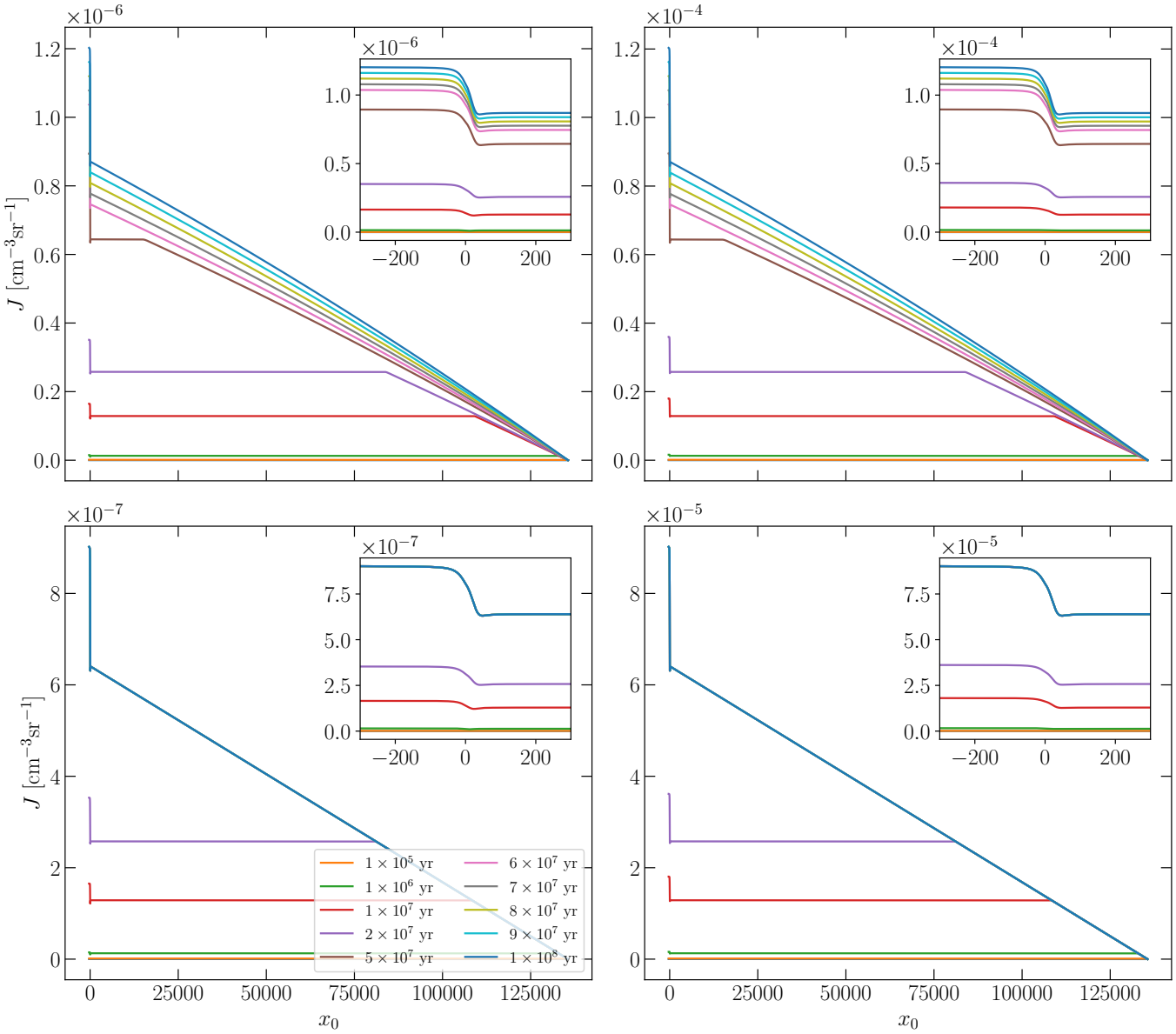

Figure 1. We show the evolution of intensity profiles for Lyα continuum + 20% injected photons for 100 Myr. The left (right) panels correspond to $C = 1 \times 10^{-16}$ cm^{-3} s^{-1} sr^{-1} ($C = 1 \times 10^{-14}$ cm^{-3} s^{-1} sr^{-1}). The following initial conditions are used: $z = 20$, $T = 10$ K, fully neutral H I gas; the grid on the x-axis corresponds to the variable: $x_0 = x(T = 10\ \mathrm{K})$. The evolution of the profile close to $x = 0$ is shown in the inset. The bottom panels assume local approximation. In this approximation, the expansion rate and the number density of H I atoms are held fixed to their initial value for solving Equations (2), (5), (6), and (7). If this evolution is switched off, a quasi-static equilibrium is reached after nearly 50 Myr. The top panels, the realistic case in which all relevant quantities are allowed to evolve, show a slow change of the photon profile even at late times.

4 orders of magnitude variation in the heating rate of the additional source and 6 orders of magnitude variation in the Lyα photon injection rates in Figure 3.

The following inferences can be drawn from Figure 3: (a) For the Lyα injection rates lower than $C \lesssim 10^{-18}$, Lyα photons have a negligible impact on X-ray heating (bottom right panel). (b) For large Lyα injection rates, $C \gtrsim 10^{-12}$, the thermal evolution of the neutral gas is largely determined by Lyα photons (the top left panel of Figure 3 should be compared to the left panel of Figure 2). (c) The main tendency of Lyα photons is to drive the coupled system to equilibrium temperature, which is nearly independent of the photon injection rate, C (Figure 2). (d) At early times, a mix of Lyα and X-ray photons can cause additional heating. However, the long-term evolution is determined by Lyα photons, preventing X-ray photons from heating the IGM.

Figure 3 shows that Lyα photons act as a sink for the additional source of heating. To understand this behavior, we briefly review the case without this additional heating. For any initial condition, the coupled system of Lyα photons and H I tends to reach an equilibrium, which drives the gas temperature and Lyα color temperature (close to the line center $x \simeq 0$) toward each other. For continuum photons, the initial color temperature is infinite, while it is zero for injected photons. This is the reason continuum photons heat while the injected photons cool. For a mix of continuum and injected photons, with the former providing the dominant contribution, we get initial heating followed by an approach to equilibrium.

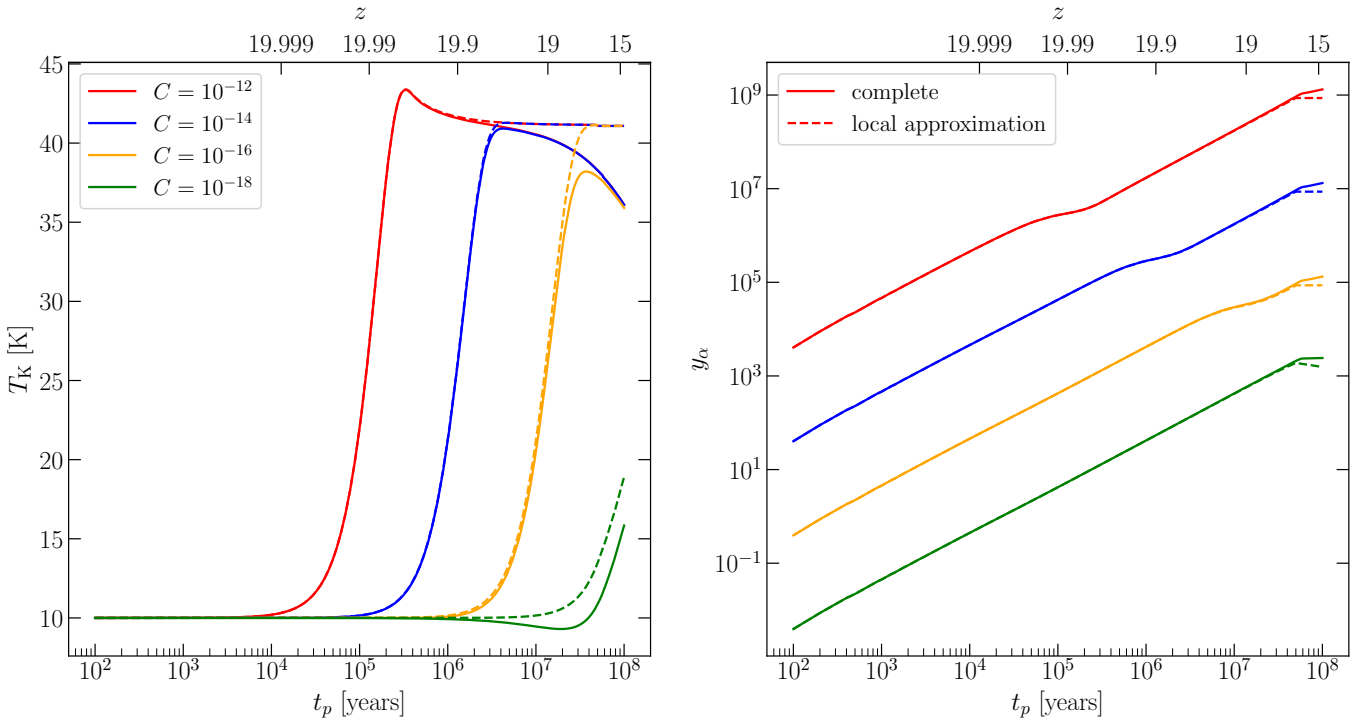

Figure 2. In the left panel, we show the thermal evolution of the gas for the photon injection model (Lyα continuum + 20% injected photons) and initial conditions as in Figure 1 for 100 Myr with different photon injection rates, C. The solid curves include all the relevant physics, while the dashed curves correspond to the aforementioned local approximation (Figure 1). In local approximation, a quasi-static thermal equilibrium is reached, while a slow evolution of the gas temperature is seen in the other case. For a very small value of C, the temperature initially decreases due to adiabatic cooling before the Lyα intensity builds up. In the right panel, we show the evolution of the coupling coefficient y_α for the same cases. y_α is proportional to $J(\nu_\alpha)$ and inversely proportional to T_α (Equation (4)). Initially, y_α increases rapidly as $J(\nu_\alpha)$ (or equivalently $J(x = 0)$) increases rapidly (Figure 1). If the temperature also increases sharply (left panel), y_α flattens. Over longer times, after the tilted profile is reached, $J(0)$ is nearly constant, but the temperature decreases slightly, leading to a small increase in y_α. In local approximation, y_α reaches a constant as both $J(0)$ and the temperature reach steady state values (left panel and Figure 1).

We next try to determine the details of the dynamics of the coupled system when an additional source of heating of the gas is switched on:

(a) First, we qualitatively discuss what we expect when the Lyα photons and the neutral gas are already in thermal equilibrium with each other, owing to Compton and inverse Compton scattering close to the line center. In this case, if either of the components receives additional energy, it would be shared with the other as the system attempts to reach a new equilibrium state. For instance, if continuum photons are added, the gas would heat as these photons have an excess of blueward photons over the equilibrium state. Similarly, the addition of injected photons, which have an excess of redward photons, causes the gas to cool as energy is transferred from the gas to photons in reaching the new equilibrium (for details see Paper I). For the same reason, if the gas is heated (e.g., by X-ray photons), a fraction of the additional energy is absorbed by Lyα photons. The magnitude of this fraction is determined by the relative heat capacities of the two components. The results shown in Figure 3 are compatible with this qualitative understanding. However, for the general case we consider, it is not possible to gain analytic insight into this process. Therefore, we consider a simpler case—no expansion and no photon pumping ($H = C = 0$)—to get a clearer understanding.

(b) For the simpler case, as shown in Paper I, Compton and the inverse Compton scattering relax the coupled system to a thermal equilibrium with a common temperature T_K, and the spectrum of the radiation in equilibrium is $J(x) \propto \exp(2\eta x) = \exp(-h(\nu - \nu_\alpha)/kT_K)$.[4]

(c) For this setting, we first assume the coupled H I–Lyα system to be in thermal equilibrium at $T = T_1$. Then an energy ΔE (per neutral atom) is injected into the gas. If the gas was not coupled to Lyα photons, this energy injection would raise the temperature of the gas by $\Delta T = \Delta E/k$. However, for the coupled system, this energy would be shared between the two components, and a new equilibrium temperature of the coupled system would be smaller than the one without Lyα photons.

(d) To compute the new equilibrium temperature T_2, we first note that the equilibrium spectrum of radiation is flatter close to the line center, as $T_2 > T_1$ or there are more photons on the blueward side of the line center as compared to the equilibrium at a smaller temperature. These photons are transferred from the redward to the blueward side by inverse Compton scattering as the gas is heated.

(e) The thermal energy of photons (close to the line center) is $\int h(\nu - \nu_\alpha) 4\pi J(x) dx$. This allows us to compute the amount of energy absorbed by the Lyα photons in a small volume ΔV: $\Delta E_\alpha = q n_\alpha(0) k (T_2 - T_1) \Delta V$. Here,

[4] Clearly, this spectrum cannot capture the entire picture, as it is divergent for $\nu \ll \nu_\alpha$. We discuss solutions far away from the line center in Paper I. However, this solution provides an excellent approximation even in the more general case (nonzero photon pumping and expansion) close to the line center, and as most of the energy exchange occurs close to the line center, we use it for the discussion here.

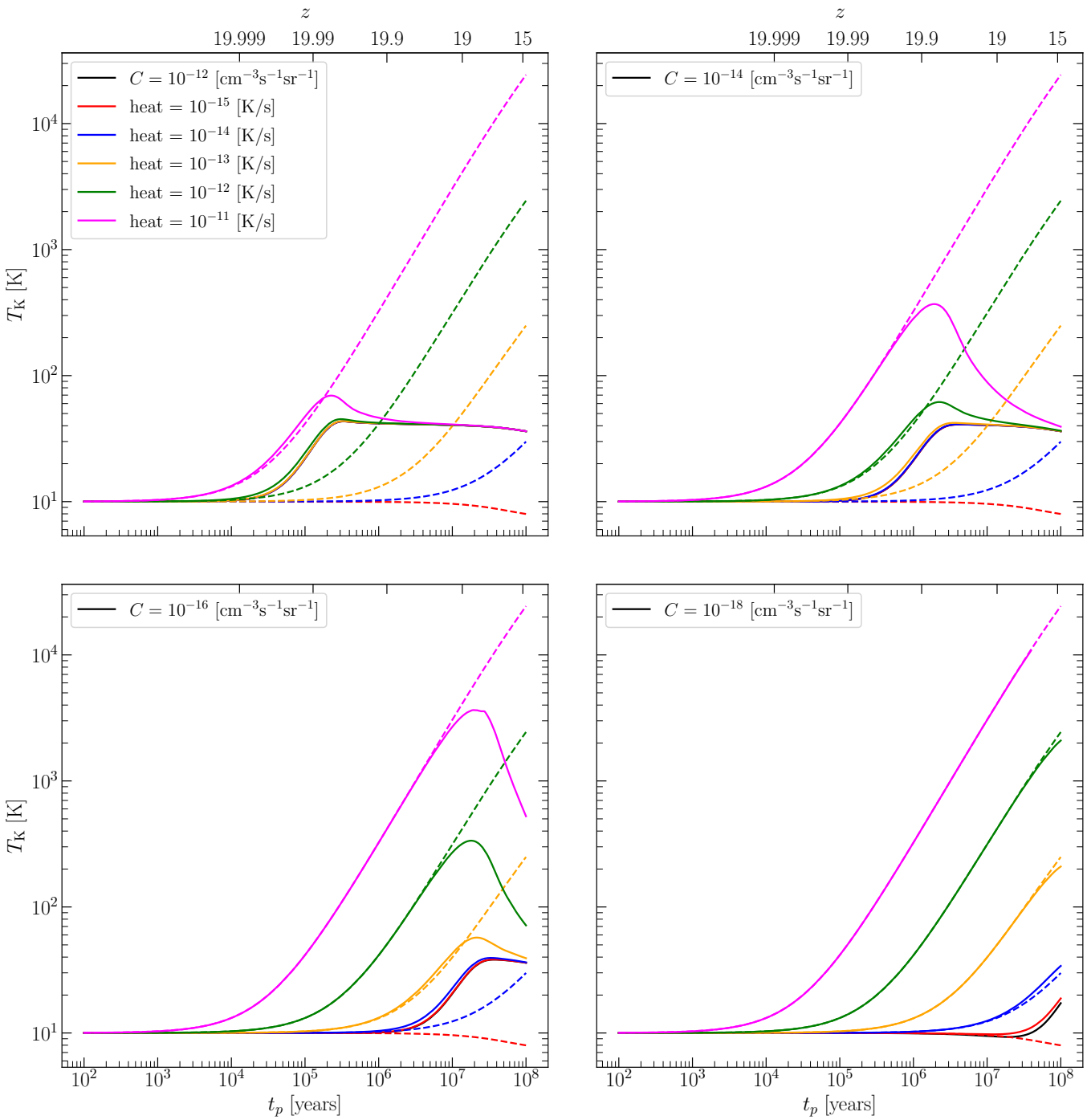

Figure 3. We show the temperature evolution of the gas, including the impact of X-ray heating. The solid lines (dashed lines) correspond to cases when the thermal effect of Lyα photons is included (excluded). The model considered is the same as in Figure 1: continuum + 20% injected Lyα photons with initial gas temperature, $T = 10$ K at $z = 20$. In each panel, the excess heating is varied over 4 orders of magnitude, while the Lyα injection rates are: $C = 10^{-12}$ cm^{-3} s^{-1} sr^{-1} (top left), 10^{-14} cm^{-3} s^{-1} sr^{-1} (top right), 10^{-16} cm^{-3} s^{-1} sr^{-1} (bottom left), and 10^{-18} cm^{-3} s^{-1} sr^{-1} (bottom right). At initial times, both X-ray and Lyα photons act as heating sources. However, the net impact of Lyα photons is to drive the system toward an equilibrium temperature, in which the gas and Lyα color temperature approach each other. This causes a fraction of the additional heat to be shared with Lyα photons, thereby preventing the X-ray photons from heating the medium. For most models shown in the four panels, this behavior is seen, with the equilibrium reaching faster for larger C. Only for $C = 10^{-18}$, the impact of Lyα photons is negligible.

$n_\alpha(0)$ is the number density of Lyα photons at the line center, and q is a number whose exact value depends upon the limit of integration; it is on the order of unity. The gas absorbs the energy $\Delta E_g = n_b k(T_2 - T_1)\Delta V$. The new equilibrium temperature is computed by equating the injected energy with the energy absorbed by the two components: $n_b \Delta E = (\Delta E_g + \Delta E_\alpha)/\Delta V$. This gives: $T_2 = T_1 + n_b \Delta E / k(n_b + q n_\alpha(0))$.

(f) The heat capacities of the two components are proportional to their respective number densities. For $n_\alpha(0) \gg n_b$, most of the thermal energy is absorbed by Lyα photons, and the resultant temperature change is

small. If $n_\alpha(0) \ll n_b$, most of the heat is absorbed by neutral atoms.

(g) Figure 3 shows solutions of the general initial value problem: the Lyα photon injection and X-ray heating start at the same time, and the expansion of the Universe is taken into account. However, the foregoing discussion also allows us to discern the main features of the dynamics of the system in this case. For small C, the temperature of the gas keeps rising owing to continuous injection of energy from X-ray photons.[5] In this limit, $n_\alpha(0) \lesssim n_b$, and the thermal evolution of the gas is nearly independent of the presence of Lyα photons. However, owing to strong thermal coupling between the two components, the Lyα spectrum close to $x \simeq 0$ evolves rapidly to establish equilibria for different temperatures. As C is increased, the temperature evolution flattens, reaches a peak, and then is driven to a fixed temperature. This is owing to several factors, which are linked to the thermal evolution without any additional heating (Figure 2), and, for this range of C, an increasingly larger fraction of the heat is absorbed by Lyα photons. For even larger C, after initial heating, the system relaxes to a quasi-equilibrium temperature and remains close to it during the later evolution of the system. This behavior is nearly independent of the heating rate because these cases correspond to $n_\alpha(0)/n_b \gg 1$.[6]

(h) Finally, a comparison of Figures 2 and 3 allows us to gauge the net impact of additional heating. For small C, the thermal evolution for the gas with and without additional heating is quite different. This is expected based on our discussion. As C is increased, the thermal evolution of the gas begins to resemble the trajectory without X-ray heating, and for large C, the thermal evolution is nearly independent of the additional heating, which is expected as $n_\alpha(0)/n_b \gg 1$ in these cases.

In the next section, we explore this issue further for more realistic models of Lyα photon injection and X-ray heating.

4.1. Lyα and X-Ray from Ionizing Sources

In the foregoing, we considered Lyα injection and X-ray heating rates over a large range of values, but we did not consider cases where they arise from the same set of sources. This is our expectation in a more realistic setting. In the literature, multiple models have been considered that simultaneously treat ionization, Lyα injection, and X-rays. In this paper, we explore the analytical models considered in J. Raste & S. Sethi (2019). In these models, the excursion set formalism is used to calculate the collapse fraction ($f_{\rm coll}$) and the volume-averaged ionization fraction ($x_{\rm H\ II}$) as a function of the redshift (S. R. Furlanetto et al. 2004). The same sources cause injection of X-ray and Lyα photons into the medium (e.g., J. Raste & S. Sethi 2018 and J. Raste & S. Sethi 2019 for details; while these papers considered the inhomogeneities of these radiation fields to compute the fluctuating component of H I signal, we are only using volume-averaged quantities in this paper as our main interest is the global H I signal). In this paper, our main focus is on the era of CD. In this era, the ionization fraction is small, and the only relevant effects arise from Lyα and X-ray photons.

The dynamics of the system is modeled using four parameters: the ionization efficiency factor $\zeta = 7.5$, the X-ray spectral index $\alpha = 1.5$, the total number of X-ray photons emitted per stellar baryon $N_{\rm heat}$,[7] and the ratio of Lyα to hydrogen-ionizing photons emitted from the sources, f_L.[8]

We initialize Equations (2), (5), (6), and (7) at $z = 25$ and evolve Lyα profiles and the IGM temperature for 500 Myr, which means the simulations end at $z \simeq 8$. We show these results in Figure 4. We only vary $N_{\rm heat}$ and f_L in displaying our results, as the results are robust to changes in the other two parameters.[9]

We first analyze the case where the X-ray heating rate is low (the lower left panel of Figure 4). In this case, the net thermal impact of Lyα photons is to heat the system. This, as noted above, is expected and consistent with the results shown in Figure 2. However, in the middle and top left panels, in which the X-ray heating rates are larger, the Lyα photons prevent heating. This is in line with the discussion on Figure 3. The most important result of the analysis, already anticipated in Figure 3, is that in all cases, for a large enough f_L, the temperature reaches an equilibrium value, which is close to the equilibrium temperature reached without X-ray heating (Figure 2). This equilibrium temperature is entirely determined by the ratio of injected to continuum photons (for details, see Paper I). In Figure 4, we assume the fraction of injected photons to be 20%, which is close to the value expected from the quantum mechanics of the photon cascade and the spectrum of ionizing sources (e.g., L. Chuzhoy & P. R. Shapiro 2006, 2007; S. R. Furlanetto & J. R. Pritchard 2006; C. M. Hirata 2006). L. Chuzhoy & P. R. Shapiro (2007) argued that the ratio of injected to continuum photons depends on the temperature of ionizing sources. For hot sources, the ratio reaches 0.17, and it is expected to be greater than 0.1 for cooler sources. This motivates the range we consider in the next section (Figures 4 and 5).

There are two more contributions to injected photons that we have neglected in the paper. (a) Recombination photons from ionizing regions: In ionization equilibrium, each ionizing photon causes a recombination that finally cascades to a Lyα photon.[10] This contribution is expected to be negligible for

[5] It is instructive to compare different timescales. The energy redistribution owing to inverse Compton scattering is the shortest. The X-ray heating timescale is shorter than the expansion timescale, which means the adiabatic cooling does not play an important role in Figure 3.

[6] In Figure 1, $n_\alpha(0) \simeq 10 n_b$ for $C = 10^{-16}$ and $t \gtrsim 50$ Myr. The figure also shows $n_\alpha(0)$ scales nearly linearly with C, and therefore $n_\alpha(0)/n_b \gg 1$ is achieved for most models of Lyα injection rates we consider in Figure 3.

[7] Comparing the definition of $N_{\rm heat}$ with another parameterization of X-ray heating, $\zeta_{\rm X}$, the number of photons per solar mass in stars (used in the publicly available code 21cmFAST; A. Mesinger et al. 2011), we get $N_{\rm heat} \simeq \zeta_{\rm X} m_p$. Hence, $N_{\rm heat} = 1$ would approximately correspond to $\zeta_{\rm X} = 1.2 \times 10^{57}\, M_\odot^{-1}$.

[8] In the first part of the paper, we used a constant rate of Lyα photon injection, parameterized by C. It is not straightforward to relate f_L to C as the Lyα injection rate is time-dependent for a given f_L, which translates to a changing C. For $f_L = 10^4$, $C = \{6 \times 10^{-18}, 4 \times 10^{-17}, 6 \times 10^{-17}\}$ at redshifts $z = \{20, 15, 12\}$, respectively.

[9] While modeling the impact of Lyα and X-rays, it should be noted that Lyα photons travel much further into the medium (a few hundred Mpc; e.g., J. Raste & S. Sethi 2019 for details and further references). For the purposes of this paper, we assume that all the Lyα photons emitted from the source are absorbed instantaneously; this gives us consistency with our notation in the earlier section. While such an assumption could have a major impact on the fluctuating component of the H I signal (e.g., J. Raste & S. Sethi 2019), its main impact for our purposes is to cause a sharper rise of Lyα intensity initially, close to $z \simeq 25$, but the temperature evolution (and the global H I signal) at lower redshifts is not affected.

[10] The recombination timescale for redshifts of interest could be around one-tenth of the expansion timescale, so recombination is not that efficient. However, we will assume it here for our estimates.

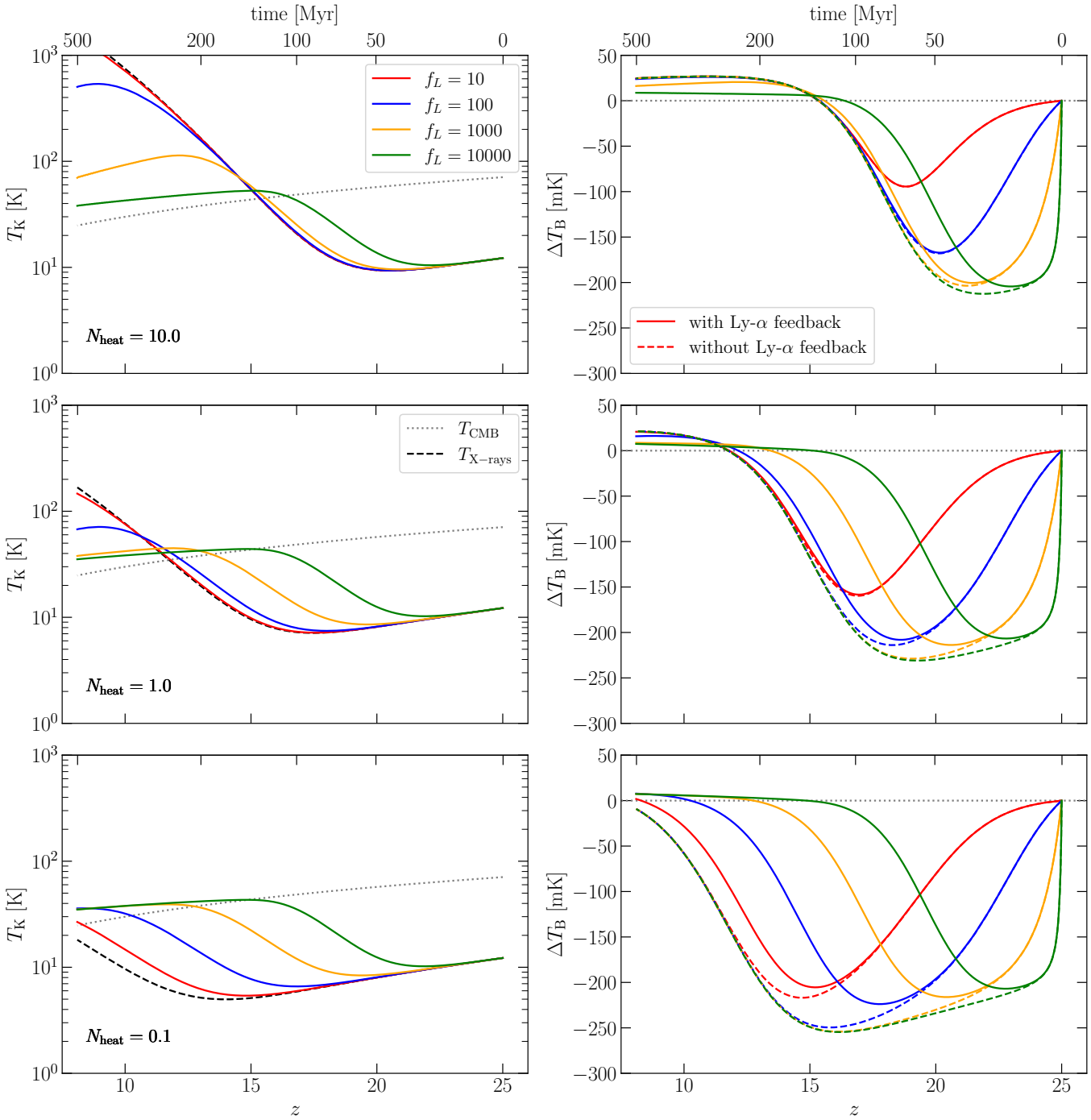

Figure 4. We show the temperature evolution of the gas (left panels) and the global 21 cm signal (right panels) for the models parameterized by $N_{\rm heat}$ and f_L (see the text for details). The Lyα model corresponds to continuum + 17% injected photons. In each panel, we fix $N_{\rm heat}$ and vary f_L by several orders of magnitude: $N_{\rm heat} = 10$ (top panel), 1 (middle panel), and 0.1 (bottom panel). Left panels: Thermal history is displayed with (solid curves) and without (dashed curve) the thermal effects of Lyα photons. These results are in agreement with thermal histories shown in Figure 3, even though the system is evolved for 500 Myr here. Right panels: The global H I signal is displayed (Equation (8)). There are two curves (solid and dashed) for each model (fixed f_L and $N_{\rm heat}$). For dashed curves, Wouthuysen–Field coupling is included (Equation (2) and the right panel of Figure 2), but not the thermal impact of Lyα photons. Solid curves include all the relevant physics of Lyα photons. For small values of f_L (small number density of Lyα photons), there is a negligible difference between the solid and dashed curves. For higher values of f_L, the inclusion of Lyα thermal effect causes the gas to heat faster initially. However, Lyα photons prevent the gas temperature from rising above the equilibrium temperature for the corresponding Lyα model (continuum + 17% injected photons), which is close to 40 K.

$f_L \gg 1$, (b) H I excitations from X-ray photons: Through secondary excitations, a single X-ray photon can excite multiple hydrogen atoms. Up to 30% of the energy of X-ray photons could be spent in exciting hydrogen atoms (e.g., J. M. Shull & M. E. van Steenberg 1985; A. Venkatesan et al. 2001). We have checked that this contribution to the injected photon budget is also negligible for our models, and it is generally smaller than the contribution from recombination photons.

We can approximate these contributions by neglecting the expansion of the Universe, varying rates of different physical processes, etc. If the ionized fraction of the IGM is $f_{\rm ion}$, we expect the number density of hydrogen-ionizing photons, $n_{\rm ion} \simeq q n_b f_{\rm ion}$; here $q \simeq 10$ takes the impact

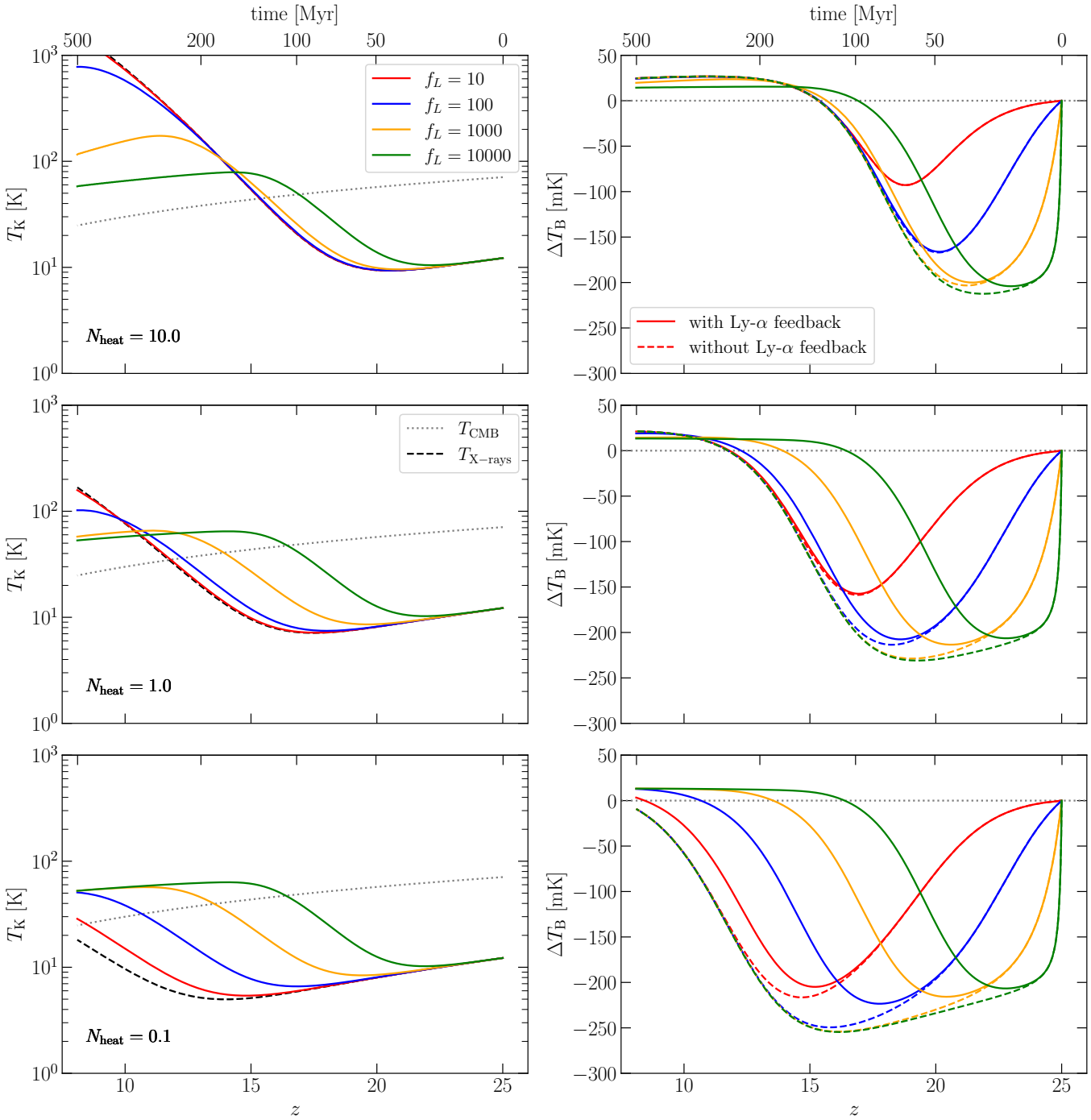

Figure 5. The same as Figure 4, but for the Lyα model, continuum plus 10% injected photons. The equilibrium temperature in this case is $T \simeq 70$ K, which gives the redshift of crossover of the global H I signal from absorption to emission, $z_c \simeq 17.5$.

of recombination into account. We know that nearly 20% of X-ray photon energy goes to heat the mostly neutral medium. For simplicity, let us assume all X-ray photons have the same energy E. Nearly 30% of the energy of this photon goes into the excitation of the hydrogen atom to the first excited state, or each X-ray photon produces $m = pE/E_\alpha$ injected photons; here $p = 0.3$ and $E_\alpha = 10.2$ eV is the energy of the Lyα transition. If the medium is heated to a temperature T, we expect: $fn_xE \simeq (1 - f_{\rm ion})n_b kT_{\rm K}$; here $f = 0.2$ and n_x is the number density of X-ray photons. Hydrogen-ionizing photons ionize regions close to ionizing sources. The number of injected photons created by recombination in ionized regions ($N_{\rm ion}$) and by X-ray excitations in neutral regions ($N_{\rm neu}$) can now be computed. This gives us: $N_{\rm neu}/N_{\rm ion} \simeq (n_x m)/n_{\rm ion} \simeq (1 - f_{\rm ion})\, pkT_{\rm K}/(fE_\alpha q f_{\rm ion})$. Notice that this ratio is independent of the energy of X-ray photons. Using numbers suitable for our study, $T_{\rm K} \lesssim 1000$ K and $f_{\rm ion} \simeq 0.1$, we can show that $N_{\rm ion}/N_{\rm neu} \ll 1$.

As shown in Paper I, the equilibrium temperature is higher/lower for a lower/higher fraction of injected photons. The constancy of the final temperature irrespective of X-ray heating has important implications for the H I signal from CD/EoR eras, which we discuss next.

4.2. Implications for the 21 cm Signal

The observable global H I signal, the difference of H I brightness temperature and CMB temperature, can be expressed as (e.g., P. Madau et al. 1997; P. A. Shaver et al. 1999; N. Y. Gnedin & P. A. Shaver 2004; S. K. Sethi 2005; J. R. Pritchard & A. Loeb 2012; J. Raste & S. Sethi 2019):

$$\Delta T_b \simeq 26.25 x_{\rm H\,I}\left(1-\frac{T_{\rm CMB}}{T_{\rm S}}\right)\left(\frac{1+z}{10}\right)^{1/2} \times\left(\frac{0.14}{\Omega_m h^2}\right)^{1/2}\left(\frac{\Omega_b h^2}{0.022}\right)\,{\rm mK}. \quad (8)$$

This signal is determined by the evolution of spin temperature, $T_{\rm S}$, which is given by Equation (2); $T_{\rm S}$ is determined simultaneously with Equations (5), (6), and (7). The system of equations is initialized at $z = 25$ with the matter temperature $T_{\rm K} \simeq 10$ K (left panels of Figure 4), which corresponds to the post-recombination, unheated gas (for details, see, e.g., J. Raste & S. Sethi 2018 and references therein). The global H I signal, corresponding to the thermal history given in the left panels, is displayed in the right panels of Figure 4. The lower right panel shows the case when X-ray heating is small. In this case, as already noted, the net impact of Lyα photons is to provide heating in addition to X-ray photons, which, it follows from Equation (8), means the H I signal is shallower in absorption. In the other two cases, the net impact of Lyα photons is to provide initial heating followed by cooling.

The most striking feature of the H I signal in all three panels occurs in the limit when Lyα photon density becomes large. In this case, as discussed above, the system relaxes to an equilibrium temperature, which is independent of both the Lyα photon density and the heating rate. As $T_\alpha \simeq T_{\rm K}$ and $y_\alpha \gg 1$ (right panel of Figure 2), from Equation (2) it follows that $T_{\rm S} \simeq T_{\rm K}$. This means that for a given neutral fraction, $x_{\rm H\,I}$, the global H I signal is frozen to a pattern that is independent of both Lyα photon intensity and the X-ray heating rate. During the CD, $x_{\rm H\,I} \simeq 1$, and Equation (8) shows that the global H I signal is entirely determined by $T_{\rm S}$ during this era. As $T_{\rm S}$ is known in the limit of large Lyα photon density, the redshift, z_c, at which the global H I signal makes a transition from absorption to emission is also fixed. For the injected to the continuum ratio we consider in Figure 4, $T_{\rm S} \simeq 40$ K, which, from Equation (8), gives $z_c \simeq 13$. During the EoR, $x_{\rm H\,I}$ varies substantially and finally vanishes. Therefore, by fixing $T_{\rm S}$, we cannot determine ΔT_b during this era. However, as $x_{\rm H\,I} < 1$, we obtain an upper limit on the H I signal. In Figure 5, we consider a different model of Lyα injection (continuum plus 10% injected photons). The most notable difference between Figures 4 and 5 is the equilibrium temperature for a large Lyα photon density. As expected and shown in Paper I, the equilibrium temperature is higher for a smaller fraction of injected photons. In the case shown in Figure 5, the equilibrium temperature is close to 70 K, which gives $z_c \simeq 17.5$. All features of the global H I signal shift to higher redshifts in this case.

The previous paragraph summarizes the most important outcome of our analysis. Our study shows that, for high Lyα injection rates, the global H I signal is greatly simplified. Figure 4 further demonstrates that the thermal impacts of Lyα and X-ray photons are coupled, and treating them as uncoupled photon fields, as is usually the case, does not treat the effect of either adequately.

Generally, the H I global signal is more complicated. Equation (8) shows that for intermediate values of photon injection rates, the H I signal is not fully fixed. Here, the main impact of Lyα photons is still to drive the gas temperature to the equilibrium temperature, which causes a decrease in the H I signal in both absorption and emission. In such cases, it is not possible to fix the redshift of crossover from absorption to emission. For lower Lyα injection rates ($C \lesssim 10^{-18}$), the thermal impact of Lyα photons is negligible, and the Lyα–X-ray system can be treated as uncoupled (Figures 3 and 4). However, even in this case, it is possible to couple the H I spin temperature to the kinetic temperature (this requires $y_\alpha \gg 1$, Equation (2)) on timescales shorter than the expansion timescale (right panel of Figure 1). This shows that a parameter space exists in which Lyα photons can play their traditional role, $T_{\rm S}$–$T_{\rm K}$ coupling, without any significant thermal impact.

5. Summary and Conclusions

In this paper, we extend our work from Paper I, which was mainly a theoretical study. In Paper I, we solved the thermal evolution of the coupled Lyα–H I gas system as an initial value problem. In this paper, we carry out necessary improvements to our earlier analysis and demonstrate the relevance of our work for the H I signal during CD.

Our main results can be summarized as follows:

(1) *Long-term evolution of photon profile and gas temperature*. The photon profile stops evolving on long enough timescales if the expansion of the Universe is neglected. The timescale over which this equilibrium is reached depends on $x_{\rm max}$ and is around 50 million years for the realistic case considered in this paper. With the inclusion of expansion, the photon profile evolves more rapidly during the flat profile phase but slowly after the tilted profile phase is reached Figure 1). For more details on the transition from flat to tilted profile and approach to equilibrium, see Paper I. The long-term evolution of gas temperature shows that, when the expansion is neglected, an equilibrium is reached on a timescale that varies inversely with photon injection rate C (left panel of Figure 2). As shown in Paper I, the equilibrium temperature is independent of the photon injection rate and depends only on the ratio of injected to continuum photons. The long-term thermal evolution shows a slow decrease at $t \gtrsim 10$ Myr owing to the expansion of the Universe.

(2) *X-rays as an additional heating source*. We expect X-rays from accretion around the first sources to heat the neutral IGM around ionized regions during the CD/EoR eras. We include this effect in addition to the thermal impact of Lyα. In the literature, these two are treated as uncoupled. However, our analysis shows that Lyα photons–H I gas–X-ray photons constitute a strongly coupled system in the limit when the Lyα injection rates are large. As shown in Figure 3, both Lyα and X-ray photons heat at early times, so they act as uncoupled sources of heat. This behavior is also seen when the injection rate is low ($C = 10^{-18}$). At longer times and large injection rates, the next impact of Lyα photons is to prevent X-ray heating. For large C, the system is driven toward an equilibrium temperature that is solely

determined by Lyα photons (Figure 2). Our result underlines the importance of treating the issue as an initial value problem and as a coupled system. While our analysis suggests a major rethink on how this coupled system is treated, it is not needed for small injection rates, $C \lesssim 10^{-18}$. In this case, Lyα photons make a negligible thermal impact (Figure 3) and are not coupled to X-ray heating (Figure 4). However, even in this case, the Wouthuysen–Field effect efficiently couples the hyperfine H I level to the gas temperature as one reaches $y_\alpha \gg 1$ over timescales shorter than the expansion timescales (right panel of Figure 2).

(3) *H I signal*. For computing the H I signal, we consider specific reionization models in which ionizing, Lyα, and X-ray photons are emitted by the same sources. The thermal histories and the global H I signal for these models are shown in Figure 4. For a small Lyα injection rate, Lyα acts as an independent heating source, which makes the H I signal during the CD era shallower. The distinguishing feature of our analysis arises again when the Lyα injection is large. As the gas temperature gets frozen in this case, this completely determines: (a) the H I signal during the CD era when $x_{\rm H\ I} \simeq 1$ and (b) the crossover redshift from absorption to emission. These features depend only on the ratio of injected to continuum photons. This is the most important result of our analysis.

In our analysis, we assume two models of Lyα injection: (a) a source with a constant injection rate C (Figure 3), and (b) a model based on sources of ionization that switch on at $z = 25$ (Figures 4 and 5). How robust are our results to more complicated evolution histories of Lyα injection? As discussed above and also in Paper I, our results are mainly determined by the injection rate of Lyα photons and their number density and are therefore relatively insensitive to other complications. One case in which our results might radically alter is if the Lyα source is turned off. This causes the medium to heat for the following reason: injected photons, which are responsible for cooling, redshift away from the resonance on short timescales ($t \lesssim 0.1$ Myr, see Paper I for details) while continuum photons continue redshifting into the resonance from the blueward side for $t \simeq 100$ Myr. The continuum photons, even as their number gets diluted owing to the change in redshift, continue heating the medium over this timescale before the tilted profile is reached (Figure 1 and Paper I). While it is possible to build models in which ionizing sources are switched off, e.g., if the haloes responsible for ionization are molecular hydrogen-cooled and they are destroyed by Werner band photons from these sources (e.g., R. Barkana & A. Loeb (2001) and references therein), we expect the atomic-cooled haloes to dominate the reionization process for $z \lesssim 15$–20 and their number is expected to increase. In summation, our model captures the essence of relevant processes needed to understand the physical setting we consider.

There are multiple ongoing experiments to detect the global H I signal (EDGES, J. D. Bowman et al. 2018; SARAS, S. Singh et al. 2022; REACH, E. de Lera Acedo et al. 2022; LEDA, D. C. Price et al. 2018; PRIzM, L. Philip et al. 2019; MIST, R. A. Monsalve et al. 2024). Most of these experiments target a range of frequencies that cover the redshift range $7 < z < 20$. Generally, these experiments search through thousands of global H I signal templates to determine the parameterized theoretical model. Figures 4 and 5 capture the diversity of the global H I signal. However, as already noted above, our work makes a definitive prediction if the Lyα photon density reaches large values at early times. In this case, the temperature of the medium becomes nearly independent of the heating rate. Figures 4 and 5 partially capture this limit, but it is seen more clearly in Figure 3 for larger values of C. In this limit, the global H I signal can be determined during the era of CD. Such a signal would be easier to search for, e.g., in terms of three parameters: the crossover redshift z_c, the depth of the signal for a fixed redshift $z > z_c$, and the height of the signal for a fixed redshift $z < z_c$. For an injected-to-continuum photon ratio in the range between 0.10 and 0.17, as expected from theory (e.g., L. Chuzhoy & P. R. Shapiro 2007), $17.5 < z_c < 13$ (Figures 4 and 5). This means that the global H I signal might be able to determine this ratio, which depends on the quantum mechanics of the hydrogen atom and some properties of the ionizing sources.

Acknowledgments

We would like to thank the anonymous referee for useful comments and suggestions, which helped us improve this paper.

ORCID iDs

Janakee Raste https://orcid.org/0000-0001-7451-6139

References

Barkana, R., & Loeb, A. 2001, PhR, 349, 125
Becker, G. D., D'Aloisio, A., Christenson, H. M., et al. 2021, MNRAS, 508, 1853
Becker, R. H., Fan, X., White, R. L., et al. 2001, AJ, 122, 2850
Bosman, S. E. I., Davies, F. B., Becker, G. D., et al. 2022, MNRAS, 514, 55
Bowman, J. D., Rogers, A. E. E., Monsalve, R. A., Mozdzen, T. J., & Mahesh, N. 2018, Natur, 555, 67
Chen, X., & Miralda-Escudé, J. 2004, ApJ, 602, 1
Chugai, N. 1980, SvAL, 6, 91
Chuzhoy, L., & Shapiro, P. R. 2006, ApJ, 651, 1
Chuzhoy, L., & Shapiro, P. R. 2007, ApJ, 655, 843
de Lera Acedo, E., de Villiers, D. I. L., Razavi-Ghods, N., et al. 2022, NatAs, 6, 984
Fan, X., White, R. L., Davis, M., et al. 2000, AJ, 120, 1167
Field, G. B. 1958, PIRE, 46, 240
Furlanetto, S. R., Oh, S. P., & Briggs, F. H. 2006, PhR, 433, 181
Furlanetto, S. R., & Pritchard, J. R. 2006, MNRAS, 372, 1093
Furlanetto, S. R., Zaldarriaga, M., & Hernquist, L. 2004, ApJ, 613, 1
Ghara, R., & Mellema, G. 2020, MNRAS, 492, 634
Gnedin, N. Y., & Shaver, P. A. 2004, ApJ, 608, 611
Hassan, S., Lovell, C. C., Madau, P., et al. 2023, ApJL, 958, L3
Hinshaw, G., Larson, D., Komatsu, E., et al. 2013, ApJS, 208, 19
Hirata, C. M. 2006, MNRAS, 367, 259
Kulkarni, G., Keating, L. C., Haehnelt, M. G., et al. 2019, MNRAS, 485, L24
Madau, P., Meiksin, A., & Rees, M. J. 1997, ApJ, 475, 429
Meiksin, A. 2006, MNRAS, 370, 2025
Meiksin, A., & Madau, P. 2021, MNRAS, 501, 1920
Mesinger, A., Furlanetto, S., & Cen, R. 2011, MNRAS, 411, 955
Mittal, S., & Kulkarni, G. 2021, MNRAS, 503, 4264
Mittal, S., Kulkarni, G., & Garel, T. 2024, MNRAS, 535, 1979
Monsalve, R. A., Altamirano, C., Bidula, V., et al. 2024, MNRAS, 530, 4125
Morales, M. F., & Wyithe, J. S. B. 2010, ARA&A, 48, 127
Munoz, J. B., Qin, Y., Mesinger, A., et al. 2022, MNRAS, 511, 3657
Natarajan, A., & Yoshida, N. 2014, PTEP, 2014, 06B112
Philip, L., Abdurashidova, Z., Chiang, H. C., et al. 2019, JAI, 8, 1950004
Planck Collaboration, Aghanim, N., Akrami, Y., et al. 2020, A&A, 641, A6
Price, D. C., Greenhill, L. J., Fialkov, A., et al. 2018, MNRAS, 478, 4193
Pritchard, J. R., & Furlanetto, S. R. 2006, MNRAS, 367, 1057
Pritchard, J. R., & Loeb, A. 2012, RPPh, 75, 086901
Raste, J., Kulkarni, G., Keating, L. C., et al. 2021, MNRAS, 507, 4684
Raste, J., Sarkar, A. K., & Sethi, S. K. 2024, ApJ, 976, 236
Raste, J., & Sethi, S. 2018, ApJ, 860, 55

Raste, J., & Sethi, S. 2019, ApJ, 876, 56
Reis, I., Fialkov, A., & Barkana, R. 2021, MNRAS, 506, 5479
Rybicki, G., & Hummer, D. 1994, A&A, 290, 553
Rybicki, G. B. 2006, ApJ, 647, 709
Rybicki, G. B., & dell'Antonio, I. P. 1994, ApJ, 427, 603
Semelin, B., Mériot, R., Mertens, F., et al. 2023, A&A, 672, A162
Sethi, S. K. 2005, MNRAS, 363, 818
Shaver, P. A., Windhorst, R. A., Madau, P., & de Bruyn, A. G. 1999, A&A, 345, 380
Shimabukuro, H., Hasegawa, K., Kuchinomachi, A., Yajima, H., & Yoshiura, S. 2023, PASJ, 75, S1
Shull, J. M., & van Steenberg, M. E. 1985, ApJ, 298, 268
Singh, S., Jishnu, N. T., Subrahmanyan, R., et al. 2022, NatAs, 6, 607
Venkatesan, A., Giroux, M. L., & Shull, J. M. 2001, ApJ, 563, 1
Venumadhav, T., Dai, L., Kaurov, A., & Zaldarriaga, M. 2018, PhRvD, 98, 103513
Yan, H., Ma, Z., Ling, C., Cheng, C., & Huang, J.-S. 2022, ApJL, 942, L9
Zhu, Y., Becker, G. D., Christenson, H. M., et al. 2023, ApJ, 955, 115